Probing Excited-State Electron Transfer by Resonance Stark Spectroscopy: 4. Mutations near B_L in Photosynthetic Reaction Centers Perturb Multiple Factors that Affect $B_L^* \rightarrow B_L^+ H_L^-$

Thomas P. Treynor, Chiaki Yoshina-Ishii, and Steven G. Boxer*

Department of Chemistry, Stanford University, Stanford, California 94305-5080

Received: March 5, 2004; In Final Form: May 21, 2004

Stark spectra have been obtained in the region of absorption by the accessory bacteriochlorophylls (the B-band region around 800 nm) in *Rhodobacter sphaeroides* reaction centers. The Stark spectra in this region are dominated by the resonance Stark effect of B_L, the accessory bacteriochlorophyll on the functional side; results in Part 1 of this series demonstrated that these effects are associated with the alternative electron-transfer pathway $B_L^* \rightarrow B_L^+H_L^-$, where H_L is the bacteriopheophytin acceptor on the functional side. Low-temperature absorption and Stark spectra for unmodified, Q_A-reduced and P-oxidized samples of wild-type and three mutant reaction centers (M203GD, M210YF, and M210YW) are presented. This combination samples many perturbations to the $B_L^+H_L^-$ state that can be quantified by fitting the data using the theory of resonance Stark effects developed in Parts 2 and 3 of this series. It is found that the mutations perturb not only the energy of $B_L^+H_L^-$ relative to that of B_L^* but also the electronic coupling between these states and the effective distance of charge transfer for the reaction $B_L^* \rightarrow B_L^+H_L^-$. Rates for this alternative charge-separation pathway are estimated from spectral analysis and compared with time-resolved measurements reported by several groups. By comparison of the spectra from the Q_A-reduced and P-oxidized samples, it is found that the dielectric screening is larger in the region around Q_A and the probe $B_L^+H_L^-$ than in the region around P and $B_L^+H_L^-$. The mean frequency of the vibrational modes that are coupled to this charge-transfer process is also estimated. In the context of fitting the Stark spectra, evidence is presented for a strong excitonic interaction between the localized transitions at the B_L and H_L binding sites in reaction centers containing the M214LH mutation and among the localized transitions at the B_L, B_M, and P binding sites in wild-type reaction centers.

The initial electron-transfer reaction in bacterial photosynthesis follows the electronic excitation of the chromophores in an integral membrane protein called the reaction center (RC).[1] The RC consists of three polypeptides, denoted L, M, and H, which bind six bacteriochlorins in a roughly C_2-symmetric arrangement, illustrated schematically in Figure 1. Unidirectional electron transfer from a strongly interacting pair of bacteriochlorophylls (BChls) known as the special pair or P to only one of two possible bacteriopheophytin (BPhe) acceptors, denoted H_L, occurs with a time constant of about 3 ps at room temperature.[2] Subsequent electron transfer to a nearby quinone, Q_A, proceeds with a time constant of 200 ps.[3] The monomeric BChl between P and H_L, denoted B_L, is known to assist this ultrafast charge separation on its way from P to H_L.[4] The BChl and BPhe that are related by the local C_2 axis of symmetry to B_L and H_L, denoted B_M and H_M, respectively, have not been found to participate in any electron-transfer process in wild-type (WT) RCs.

Part 1 of this series identified unusually large and broad Stark spectra in the Q_y region of WT and mutant RCs with the alternative charge-separation pathway, $B_L^* \rightarrow B_L^+H_L^-$.[5] Part 2 defined the physical picture for understanding the line shapes and magnitudes of these nonclassical Stark effects, called resonance Stark effects.[6] Part 3 refined the resonance Stark model by strengthening its theoretical and conceptual foundations and by developing methods to increase the accuracy of the quantitative results presented here.[7] The physical picture of radiationless transition theory at the heart of the resonance Stark model is illustrated in Figure 2:[8] the coupling between an excited state and a continuum of vibronically coupled states gives rise to an exponential decay of the excited state and a lifetime-broadening of the transition from the ground state; the interaction between an electric field and the electric dipole moments of these dipolar states perturbs both the peak position and line width of this transition. Figure 2 also illustrates many of the parameters in the resonance Stark model applied to the specific case where $B_L^* \rightarrow B_L^+H_L^-$. The parameter Δ_{CT} is the full width at half-maximum of the Franck−Condon weighted density of states, $\rho_{FC}(\bar{\nu})$, for the horizontal transition from B_L^* to $B_L^*H_L^-$. The parameter δ is the energy of the vertical transition between B_L^* and $B_L^+H_L^-$ reduced by Δ_{CT}: $\delta = (\bar{\nu}_0 - \bar{\nu}_{CT})/\Delta_{CT}$, where $\bar{\nu}_0$ is the energy of the vertical transition between B_L and B_L^* and $\bar{\nu}_{CT}$ is the energy of the vertical transition between B_L and $B_L^+H_L^-$. Thus $\delta = 0$ corresponds to an activationless electron transfer, and negative values of δ correspond to the Marcus normal region. The parameter $\Delta\mu_R$ is the magnitude of $\Delta\vec{\mu}_{CT}$, the difference between the electric dipole moments of $B_L^+H_L^-$ and B_L^*, reduced by Δ_{CT}: $\Delta\mu_R = \Delta\mu_{CT}/\Delta_{CT}$. The parameter f is a scalar approximation to the local field correction tensor, which accounts for a possible difference between $\vec{F}$, the externally applied electric field, and $\vec{F}_{int}$, the internal field at B_L and H_L: $\vec{F}_{int} = f\vec{F}$. The parameter W_R is the square of the electronic

* To whom correspondence should be addressed. Phone: (650) 723-4482. Fax: (650) 723-4817. E-mail: Sboxer@stanford.edu.

10.1021/jp048986c CCC: $27.50
Published on Web 08/07/2004

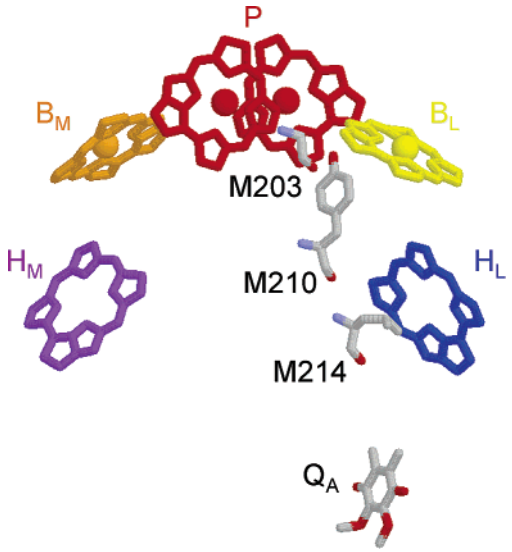

Figure 1. The organization of the reactive components in the *Rb. sphaeroides* photosynthetic reaction center and the amino acid residues M203, M210, and M214.[35] The two bacteriochlorophylls in red are closely associated forming the special pair, labeled P. The other primary colors, yellow and blue, are used for the monomeric bacteriochlorophyll, B_L, and bacteriopheophytin, H_L, which participate in the primary electron-transfer events. The remaining bacteriochlorophyll, B_M, and bacteriopheophytin, H_M, are colored orange and violet, respectively, such that the spectral ordering of the five colors that we have used for the six bacteriochlorins reflects the spectral ordering of the five principle Q_y transitions of reaction centers. Both the M203 and M210 residues are located adjacent to B_L. The M214 residue is adjacent to H_L, and its mutation to histidine substitutes a BChl, denoted β, for BPhe in the H_L binding site.

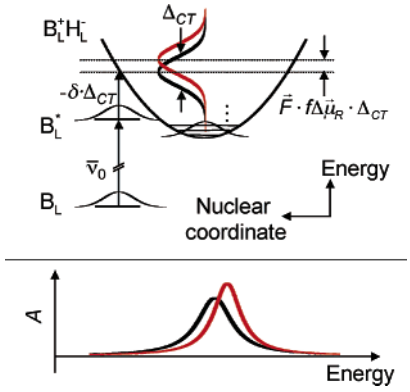

Figure 2. Resonance Stark model with labels corresponding to the reaction $B_L^* \rightarrow B_L^+H_L^-$. The transition between the B_L and B_L^* surfaces is broadened by the mixing between B_L^* and the continuum of vibronic states on the $B_L^+H_L^-$ surface. The energetic interaction of an electric field, F, with the electric dipole moment of the $B_L^+H_L^-$ state perturbs this mixing and the absorption spectrum (A) in turn, shown schematically below. Gaussians plotted as a function of nuclear coordinate represent the probability densities of the ground vibrational wave functions on each surface. Gaussians plotted as a function of energy represent the Franck−Condon weighted density of states, which describes the vibronic coupling between B_L^* and the states on the $B_L^+H_L^-$ surface.

coupling between B_L^* and $B_L^+H_L^-$, V_0, reduced by Δ_{CT}: $W_R = V_0^2/\Delta_{CT}$. The parameter ζ_{CT} is the angle between the transition moment for the $B_L^* \leftarrow B_L$ transition and the direction of $\Delta\vec{\mu}_{CT}$. The parameters Γ_0 and Γ_{Gaus} are the Lorentzian and Gaussian contributions to the absorption line shape, respectively. The functional form for $\rho_{FC}(\bar{\nu})$ is expected to be a Poisson-distributed function, $P(\bar{\nu})$, in the limit of low temperature and a Gaussian, $G(\bar{\nu})$, in the limit of high temperature;[9] the latter was previously employed to analyze measurements made at 77 K.[6] In addition to describing the effects of these parameters on the resonance Stark spectra and the expected covariances between them when fitting experimental spectra, Part 3 also derives the equations needed to convert between the radiationless transition picture of excited-state electron transfer and the more common Marcus picture.[57]

Parts 1 and 2 demonstrated that both chemical oxidation of P and mutations in the vicinity of P, B_L, and H_L significantly perturb the unusual higher-order Stark spectra of the B_L absorption band in a manner that is consistent with an effect on the energy of $B_L^+H_L^-$. These observations were used to suggest that $B_L^* \rightarrow B_L^+H_L^-$ is the process responsible for the novel Stark effect. Here we use the refinement to the theory described in Part 3 to determine quantitatively the perturbations to $B_L^* \rightarrow B_L^+H_L^-$ due to P-oxidation and Q_A-reduction for WT and the single amino acid mutants M203GD, M210YF, and M210YW of *Rhodobacter sphaeroides* RCs; both the M203 and M210 residues are located adjacent to B_L (see Figure 1), and all three mutant strains are known to slow the rate of primary charge separation.[20,21,45] Some of these samples overlap those described in Parts 1 and 2; however, improvements in sample preparation, data acquisition, and analysis lead to substantially better values of the extracted parameters. In addition, we revisit the absorption and Stark spectra of RCs with the M214LH mutation to inform the analyses of the other spectra; the M214 residue is adjacent to H_L, and its mutation to histidine substitutes a BChl, denoted β, for BPhe in the H_L binding site (see Figure 1).[30] When resonance Stark effects are fit to determine how these chemical and mutagenic perturbations affect the driving force for $B_L^* \rightarrow B_L^+H_L^-$, we find that these perturbations affect this reaction in other ways as well. These results can be used to better understand measurements made in the time domain of the dynamics of B_L^*,[2,10−18] as well as the primary charge-separation process from P* to H_L.

Experimental Section

Protein Purification and Sample Preparation. All proteins were expressed as poly(histidine)-tagged constructs and purified from cultures of *Rb. sphaeroides* as described in detail elsewhere.[19] Prior to elution of the RCs from the FPLC anion-exchange resin, LDAO detergent was exchanged for Triton X-100. After elution, the fractions with the greatest ratios of P-band intensity to H-band intensity were pooled. Following dialysis, this volume was then concentrated using Centricons (YM-30, Amicon) until the maximum OD in the B band region was 0.5−1.0 through a 25 μm path length. Samples prepared in this manner could flow easily down the sides of a microfuge tube when tipped.

Concentrated RC solutions were diluted with an equal volume of glycerol such that they produced glasses of high optical quality at cryogenic temperatures. To make Q_A-reduced (Q_A^-) RCs, one volume of glycerol-containing RC solution was degassed and mixed with two volumes of degassed 50−100 mM sodium dithionite in 50/50 glycerol/buffer. P-oxidized (P^+) RCs were prepared by mixing one volume of the glycerol-containing RC solution with an equal volume of 50/50 glycerol/buffer saturated with potassium ferricyanide. More than 95% of WT, M203GD, and M210YF RCs were oxidized by this method as judged by a comparison of the Stark effects of the P bands in neutral and oxidized RCs, while 90−95% of M210YW RCs were oxidized. These observations are consistent with P/P^+ oxidation potentials measured for these mutants.[20,21]

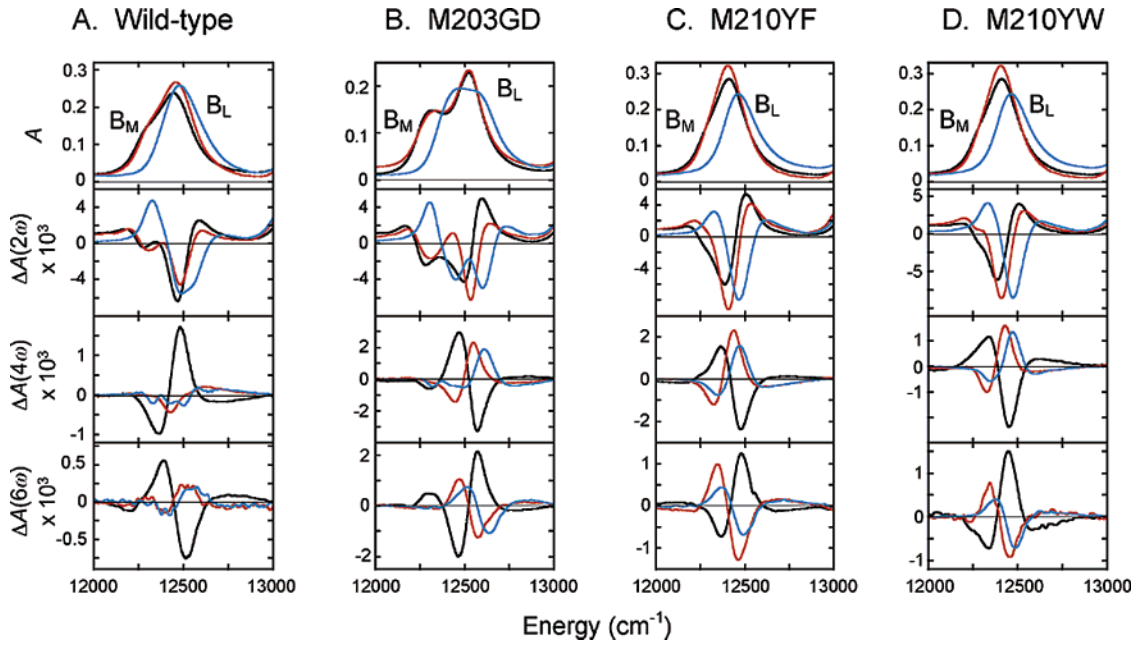

Figure 3. Absorption and Stark spectra for unmodified (black), Q_A-reduced (red), and P-oxidized (blue) preparations of wild-type (A), M203GD (B), M210YF (C), and M210YW (D). All spectra were acquired at 77 K and normalized to a field of 1 MV/cm as described in the text.

Spectroscopy. Roughly 15 μL of these solutions was placed between two glass microscope slides, each coated with a 1600 Å thick layer of indium tin oxide (ITO). The two slides were separated by an approximately 25 μm thick Kapton spacer. All samples were immersed in liquid nitrogen in a cryostat of in-house design,[22] which could maintain a bubble-free bath at 77 K for more than 5 h. This permitted longer scans, increased signal averaging, and automated data acquisition. Generally less than 2% of the light beam was depolarized along its path to the detector.

The Stark spectrometer, which also functions as a single-beam absorption spectrometer, has been described in detail elsewhere.[23] Essentially, light from a tungsten/halogen bulb is first dispersed through a monochromator, and this light is then passed through a polarizer to the sample. The ITO supports a sinusoidally oscillating voltage of frequency ω. This voltage can be as large as $\pm$2.5 kV, resulting in a field across the sample as large as 1.0 MV/cm. The light passes through the sample and is focused onto a silicon photodiode. The detector signal is wired to two different channels of a lock-in amplifier (SR830, Stanford Research Systems) to isolate both the DC component of the signal and the component that oscillates with the frequency $n\omega$, where $n = 2$, 4, or 6.

It is important to note that the time constant applied to the $n\omega$ component of the signal is much longer than the time constant applied to the DC component. Thus, whenever the wavelength of the light beam is continuously scanned, as in these experiments, this difference in time constants imparts a displacement in wavelength between these signals. This displacement increases with increasing values of either the $n\omega$ time constant or the scan rate. The narrow emissions of a mercury lamp were used to calibrate these displacements, which were typically about 2 nm for the time constants and scan rates employed. By correcting for this displacement between the $n\omega$ and DC signals, the accuracy of the $n\omega$ spectra was increased.

The 2ω and 4ω signals were acquired using a 0.4 nm scan rate and a 300 ms (24 dB bandwidth) time constant. The 6ω signals were acquired with a scan rate of 0.1 nm and a time constant of 3 s. It was found that the slowing of the scan rate greatly increased the reproducibility of the smallest 6ω signals, such as those of the WT Q_A^- and WT P^+ samples. The 2ω and 4ω signals were insensitive to these changes, except for their displacements with respect to the DC signal.

Absorption spectra from the single-beam spectrometer were not corrected for the generally flat absorption of ITO between 1000 and 700 nm or for the fluctuations in lamp intensity between scans. In some cases, improved low-temperature absorption spectra were taken with a double-beam UV/vis spectrophotometer (Lambda 12, Perkin-Elmer) on samples placed between uncoated microscope slides. Absorption spectra were baseline-corrected using the region between 1000 and 990 nm. Absorption and Stark spectra for all samples except M214LH RCs were then scaled such that they corresponded to an optical density of 0.10 at the peak of the H band, near 760 nm, for the purposes of presentation and comparison.[24] Since the perturbation to the H band in M214LH RCs is significant, the absorption and Stark spectra of M214LH RCs were scaled to an optical density of 0.105 at the peak of its P band to match the peak amplitude of the P band of WT.

To determine the value of ζ_{CT}, Stark spectra were acquired for two values of χ, the angle between the polarization vector of the light beam and the applied field. The angle χ was set to 90° by making the reflection of the beam off the sample collinear with the incoming beam. The second value of χ was determined from the increase in path length when the sample was rotated away from 90°. Since the noise of our spectrometer was detector-limited, we removed the polarizer during the acquisition of most $\chi = 90°$ spectra. These spectra were observed to be unaffected by the increase in the light at the detector apart from the increase in signal-to-noise.

Results

General Features and Improvements. Figure 3 shows the absorption, 2ω, 4ω, and 6ω spectra for WT and the three mutants (M203GD, M210YF, and M210YW) in the neutral form (black), with Q_A reduced (red), and with P oxidized (blue). Only the B band region (12 000−13 000 cm^{-1}) is illustrated. As is well-known, oxidation of P causes a larger perturbation than reduction of Q_A to the absorption spectrum in this region.[25] The

apparent narrowing of the B band upon oxidation of P is likely due to a reduction in the separation between two absorption bands commonly attributed to B_L and B_M (see below). These labels suggest that excitations are localized on individual chromophores despite much work toward characterizing the extent to which these bands might in fact be mixtures of excitations delocalized across P, B_L, B_M, H_L, and H_M.[26,27] Despite the uncertainty regarding the degree of this delocalization,[28,29] it has continued to prove useful to identify absorption features with individual chromophores, and we continue this usage here. With this in mind, it is important to note that the effects of P-oxidation and Q_A-reduction upon the integrated intensities of the B bands in Figure 3 should not be misinterpreted as due solely, if at all, to perturbations of this mixing; these intensities are also affected by normalization at the peak of the H band, itself influenced by P-oxidation and Q_A-reduction, and by small errors in the baseline due to our single-beam spectrometer. Additionally, it is possible that different preparations of RCs have resulted in different occupancies of the P, B_L, B_M, H_L, and H_M binding sites.

As described in Part 1, large, broad, and unusually shaped 4ω and 6ω Stark effects are observed for WT RCs selectively on the higher-energy side of the B band, the side associated with B_L. Also, as described in Part 1, oxidation of P to P^+ in WT RCs is observed to reduce significantly the sizes of the 4ω and 6ω spectra for the B_L band. Here we show that reduction of Q_A to Q_A^- also significantly reduces the sizes of the 4ω and 6ω spectra for the B_L band, and both have similar sizes and shapes as those in WT P^+ RCs. One notable difference between the two is that the unusual higher-order Stark effects in WT P^+ are found at higher energies than those in WT Q_A^-; this shift corresponds to a similar shift of the corresponding B_L absorption bands. As was described in Parts 1 and 2, the smaller 4ω and 6ω spectra of B_L in WT P^+ RCs can be explained by a destabilization of $B_L^+H_L^-$ due to the proximity to B_L of the positive charge on P^+, which is predicted to affect a resonance Stark effect associated with $B_L^* \rightarrow B_L^+H_L^-$ in this way.[6] Likewise, the smaller 4ω and 6ω spectra in WT Q_A^- RCs can be explained by a destabilization of $B_L^+H_L^-$ due to the proximity to H_L of the negative charge on Q_A^-. The similarities in size and shape between the 4ω and 6ω spectra of WT P^+ and WT Q_A^- suggest that the amount of this destabilization is similar for the two perturbations and that other factors that affect the resonance Stark effect of B_L take similar values as well.

Whereas the sizes of the 4ω and 6ω spectra of WT RCs change significantly due to these perturbations, the size of its 2ω spectrum does not. This is because the 2ω resonance Stark effect of the B_L band in WT RCs is either similar in size to or smaller than its 2ω classical Stark effect due to the difference between the dipole moments of the ground and excited states of this transition. The greater similarity among these 2ω spectra compared to the 4ω and 6ω spectra also suggests that the classical Stark effect of B_L is much less sensitive to these perturbations than its resonance Stark effect. Since the 4ω and 6ω resonance Stark effects in WT P^+ and Q_A^- RCs are so much smaller than those in unmodified WT RCs, it is possible that the 4ω and 6ω spectra in these cases also have contributions from other Stark effects. To gauge the sizes of any other Stark effects in this region, the absorption, 2ω, 4ω, and 6ω spectra of the B band region of RCs with the M214LH mutation (solid) are shown in Figure 4. This mutation substitutes a BChl, denoted β, for BPhe in the H_L binding site;[30] as was described in Parts 1 and 2, this substitution leads to a substantial reduction in the driving force for electron transfer to form $B_L^+\beta^-$ from B_L^*.

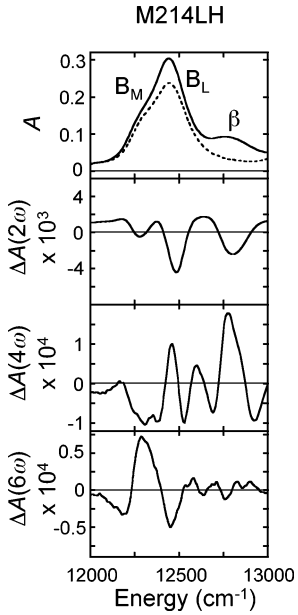

Figure 4. Absorption and Stark data for M214LH (solid) with the absorption spectrum of WT overlaid (dashed). The M214LH reaction center assembles with a BChl denoted β in the H_L binding site.

Thus, like the Stark effects of WT P^+ and WT Q_A^-, the 4ω and 6ω spectra of the M214LH mutant are much smaller compared to those of WT. Unlike the effects of the P^+ and Q_A^- perturbations, however, the effect of the M214LH mutation on the resonance Stark effect of B_L is so large that the most significant signal in its 6ω spectrum cannot even be assigned to B_L, since its center is shifted by more than 100 cm^{-1} to lower energy than the Stark effects in either WT or WT Q_A^-. This signal is an order of magnitude smaller than the 6ω signal in WT, yet it is still much larger than the 6ω Stark effects of the nearby B_L and β bands. Because this Stark effect is also much broader than these signals, we suggest that this signal is itself a resonance Stark effect. Although one might assign this resonance Stark effect to B_M, it may also be assigned to the less well characterized upper exciton band of P, which may have a small absorption in this region.[29] Regardless of this assignment, the Stark spectra of M214LH RCs indicate that the classical Stark effect of the B_L band, which is seen from the 2ω spectra in Figure 3 to be relatively insensitive to mutation, makes a substantial contribution to the 4ω spectra of WT P^+ and WT Q_A^- but not to their 6ω spectra.

In the upper panel of Figure 4, we have overlaid the absorption spectrum of WT (dashed) to illustrate evidence of mixing among the localized transitions in the RC. Whereas the small differences between the integrated intensities of the B bands of WT, WT P^+, and WT Q_A^- might be explained as artifacts as discussed above, here the difference is so large that this cannot be the case. Most of the added intensity in the B band of the M214LH mutant is concentrated on the high-energy side of the band; in fact, the two absorption spectra even follow each other closely on the low-energy side of the B band (including the P band). Since the unique absorption band at roughly 12 750 cm^{-1} in M214LH RCs cannot account for the additional intensity below it, around 12 500 cm^{-1}, these observations imply that the relative intensities of the B_M and B_L bands have been modified by the substitution of BChl for BPhe in the H_L binding site. It is implausible that this result could be due to increased occupancy of the B_L binding site in M214LH RCs since it is unlikely that this site is incompletely occupied in WT RCs; the small amplitude of the long-lived

component of fluorescence from P* is inconsistent with there being no electron acceptor in the B_L binding site of a significant fraction of WT RCs.[20] It is also unlikely that there is decreased occupancy of the P and B_M binding sites in RCs containing the M214LH mutation according to analyses of the pigment ratios for WT and M214LH RCs.[30] The increased relative amplitude of the B_L band in M214LH RCs is best explained by invoking an electronic interaction in these RCs that mixes the transitions localized on the B_L and β chromophores.

It is important to compare the spectra of WT, WT P^+, and M214LH reported here with those reported in Part 1. Whereas the line shapes of the spectra are similar in each case, the magnitudes of the 4ω and 6ω spectra, once corrected for differences in normalization, are different by factors that range between roughly $^1/_2$ and 4. These differences are likely due to improvements in sample preparation, data acquisition, and data processing between the experiments conducted for Part 1 and those conducted here. Most importantly, the WT RCs studied previously were not the SMpHis strain.[19] Since the presence of the poly(histidine) tag significantly reduces the number of steps involved in protein purification, we believe that such RCs are purified both more homogeneously and more reproducibly than RCs without the tag. Since we have found that RC preparations can be separated into P-containing and P-oxidized or P-less fractions (as judged by the presence or absence, respectively, of an absorption band attributable to P),[48] the larger ratios of P band intensity to H band intensity suggest that we have indeed achieved a greater homogeneity of P-containing RCs than previously. The increased intensity of the P band relative to the H band cannot be attributed to the presence of BChl-containing antenna proteins since P-oxidized samples of RCs have no absorption or Stark effect due to these harder-to-oxidize pigments.[32] In this regard, it is also interesting to note that the ratio of P band to H band intensity measured in a spectroelectrochemical experiment that reversibly oxidizes and reduces WT RCs[33] is both notably larger than the ratios found in many near-infrared absorption spectra of RCs in the literature and similar to that calculated from the room-temperature spectra of the WT RCs we have used here.

We have investigated the reproducibility of our current preparation procedure by obtaining 4ω and 6ω spectra for three separate preparations of WT RCs. Some variation in the line shapes and intensities of the spectra for these separate samples is observed: the largest 4ω spectrum is nearly 1.4 times as large as the smallest 4ω spectrum; the largest 6ω spectrum is nearly 1.7 times as large as the smallest 6ω spectrum. Although these differences appear to be large, the 6ω spectra are observed to increase in tandem with the 4ω spectra, so these variations can be attributed almost entirely to the roughly 10% uncertainty in the sample thickness and hence applied field,[23] as discussed below.

An important improvement in data acquisition is that we have slowed the scan rate and shortened the time constant with which spectra are acquired compared to Part 1. Whereas all spectra were previously acquired with a 0.5 nm/s scan rate and a 1 s time constant, here both the 2ω and 4ω spectra were acquired with a 0.4 nm/s scan rate and a 300 ms time constant, while the 6ω spectra were acquired with a 0.1 nm/s scan rate and a 3 s time constant. The longer time constants and faster scan rates employed previously may have reduced the size of some signals by increasing the averaging of neighboring points in the spectra. We have verified that this artifact is not present for the scan rates and time constants employed in this study. Another important improvement in data acquisition is an increased precision in the determination of the applied field strength due to better characterization of the sample thickness. For example, because the 4ω and 6ω spectra scale as approximately F^4 and F^6, respectively, an overestimation of this thickness by 10% can lead to an increase in the reported 4ω and 6ω Stark magnitudes (normalized to a field of 1 MV/cm) of 46% and 77%, respectively, and the reduced precision employed previously could account for much of the differences between the spectra.

M203GD. Figure 3B shows the absorption, 2ω, 4ω, and 6ω spectra for M203GD (black), M203GD Q_A^- (red), and M203GD P^+ (blue) samples. As was observed for WT, both the Q_A^- and P^+ perturbations to M203GD reduce the size of the 4ω and 6ω Stark spectra. The Stark spectra of M203GD Q_A^- and P^+ RCs are more similar to each other than to those of unmodified M203GD RCs, and the Stark effects of M203GD P^+ RCs are found at higher energies than those of either unmodified or Q_A^- RCs. In contrast to the 4ω spectra of either WT Q_A^- or WT P^+, those of M203GD Q_A^- and M203GD P^+ are significantly larger than the background level established by M214LH (Figure 4).

The shapes of both the 4ω and 6ω Stark spectra of M203GD Q_A^- are more similar to those of WT than to those of M203GD; although the sizes of the WT and M203GD Q_A^- spectra are somewhat different, the differences could be accounted for by the sample-to-sample variation in magnitudes noted above. Thus it may be that the effect of Q_A-reduction on the resonance Stark effect of M203GD is to offset the effects of the M203GD mutation on the resonance Stark effect of WT almost precisely. Since, as described in Parts 2 and 3, resonance Stark line shapes are sensitively determined by the reduced driving force δ and are only weakly affected by the reduced coupling W_R and the reduced difference dipole moment $\Delta\mu_R$, the observation that Q_A-reduction of M203GD yields similar line shapes to those of WT suggests that Q_A-reduction and the M203GD mutation have opposite effects on the energy of $B_L^+H_L^-$. Since we have shown above that Q_A-reduction destabilizes $B_L^+H_L^-$, the M203GD mutation likely stabilizes $B_L^+H_L^-$. This qualitative result is supported by quantitative analyses below and is inconsistent with the proposal that an aspartic acid at position M203 would donate a hydrogen bond to B_L.[20] Although qualitatively consistent with this residue being deprotonated and negatively charged, as argued for the analogous mutation in *Rhodobacter capsulatus* RCs based on resonance Raman spectra,[36] this result could also be explained by the dipole moment of the neutral residue being oriented to effect this stabilization.

An important difference between the B bands of WT and M203GD RCs is that the B_M and B_L bands are clearly resolved in the latter. With the increased resolution, it is clear that in M203GD the peak amplitude of the B_M band is considerably smaller than that of the B_L band. Thus, in M203GD, the two bands have either very different integrated intensities, very different widths, or both. As was observed for WT, the P^+ perturbation in M203GD causes an apparent narrowing of the absorption spectrum; however, since there was a greater separation between the B_M and B_L bands to begin with in M203GD, the B band of M203GD P^+ is roughly as broad as the B band of WT. However, the shapes of these bands are conspicuously different, which would not be the case if the relative amplitudes of the B_M and B_L bands in M203GD P^+ were the same as those in WT. Thus we conclude that the relative amplitudes of the B_M and B_L bands are altered either by the M203GD mutation, by the oxidation of P, or by both.

M210 Mutants. Figure 3C shows the absorption, 2ω, 4ω, and 6ω spectra for M210YF (black), M210YF Q_A^- (red), and M210YF P^+ (blue) samples. Figure 3D shows the absorption, 2ω, 4ω, and 6ω spectra for M210YW (black), M210YW Q_A^- (red), and M210YW P^+ (blue) samples. In contrast to the M203GD mutation, both the M210YF and M210YW mutations cause the B band absorption to narrow compared to that of WT. Nevertheless, an additional narrowing, as well as a shift to higher energy, is again evident upon oxidation of P. As was observed for M203GD, the resonance Stark effects in P^+ RCs are found at higher energies than those in either unmodified or Q_A^- RCs; also, for both M210YF and M210YW, the line shapes of the Stark spectra in Q_A^- and P^+ RCs are more similar to each other and to those of WT than to those in the unmodified mutant RCs. Therefore, like the M203GD mutation, the M210YF and M210YW mutations must stabilize $B_L^+H_L^-$. Unlike the 4ω and 6ω spectra of WT, M203GD, and M210YW RCs, the 4ω and 6ω Stark spectra of M210YF are not observed to decrease significantly in size upon Q_A-reduction. This difference can be attributed largely to the uncertainty in the sample thickness as described above.

It is important to note that the shapes of the 4ω and 6ω spectra reported for M210YF here are noticeably different than those reported in Part 1, yet the shapes reported for M210YF P^+ are similar. One of the explanations that we have suggested for the differences in the sizes of the 4ω and 6ω spectra for WT is applicable here as well. If the previous preparations had a mixture of P-containing and P-oxidized RCs, then the previously reported Stark spectra for the unmodified RCs should appear to be a superposition of the unmodified and P-oxidized spectra reported here. Indeed, at 77 K the ratio of the peak amplitude of P to that of H is 1.08 for the M210YF RCs used here, compared to a value of less than one for the M210YF RCs used previously;[5] moreover, it is straightforward to arrive at a shape like that reported previously for M210YF from a superposition of line shapes of the M210YF and M210YF P^+ spectra reported here. Since the WT P^+ Stark spectra are so much smaller than those of unmodified WT, a superposition of these Stark spectra should not alter the shape of the WT spectra to as large a degree; this is consistent with the observation that the shapes of the Stark spectra of WT reported here are similar to those reported previously.

Analysis

The resonance Stark line shapes for the B_L band in the M203GD and M210YW mutations, like the M210YF mutation, are consistent with stabilization of $B_L^+H_L^-$. To quantify these perturbations to the driving force for excited-state electron transfer, the resonance Stark spectra are fit to the model developed in Part 2 and refined in Part 3. As discussed in Part 3, these perturbations can be determined more accurately by increasing the accuracy of the model for the absorption spectrum. Since the M203GD absorption spectrum has the best resolution of the B_M and B_L bands, we focus first on fitting the absorption and Stark spectra of this mutant.

By fitting RC absorption spectra to a sum of two Voigt profiles, representing B_M and B_L, we make the assumptions that the contributions from the lower and upper exciton bands of P are both negligible in this region and that the B_M and B_L bands are symmetric. Although these assumptions are likely to introduce some error into the fit values of the resonance Stark parameters determined below, we argue that these errors are small. To characterize the background absorption by P in the B band region, we refer to the low-temperature absorption spectrum of the M182HL mutant.[12,66] This mutation substitutes BPhe for BChl in the B_M-binding site, resulting in a significant loss of absorption on the low-energy side of the B band and a significant increase in absorption on the high-energy side of the B band.[67] The absence of absorption by B_M in M182HL reveals that the low-energy side of its B band, including the peak near 12 500 cm^{-1}, is well described by a single, largely Lorentzian Voigt profile.[48] This result indicates that the absorption due to P in this region changes slowly with energy. Because the absorption due to P on the low-energy edge of the B band appears to be roughly 10% of the absorption at the peak of the B band, this result indicates that the absorption of P in the M182HL mutant cannot be much larger than this value in the region from 12 000 cm^{-1} to above 12 500 cm^{-1}. Although it is conceivable that the absorption spectrum of P is significantly altered by the M182HL mutation, difference spectra calculated from the low-temperature absorption spectra of M182HL and WT indicate that there is no significant change in the B band region that cannot be explained simply by the disappearance of the B_M band and the appearance of the new band.[48] This difference spectrum, which helps to resolve the intrinsic line shape of the B_M band, is itself well characterized by a sum of two Voigt profiles, indicating that the B_M band is quite symmetric in WT. The B_L band also appears to be quite symmetric, as judged by the similarities between the shapes of the low-energy side of the B band in M182HL and the high-energy side of the B band in WT.[12,66] The fit to the B band absorption of M203GD is illustrated in the upper left panel of Figure 5. It is apparent that this fit (circles) to the data (solid line) from a sum of the B_L and B_M bands (dashed and dotted lines with peak positions at 12 525 and 12 310 cm^{-1}, respectively) can account for nearly all of the absorption in the region between 12 000 and 13 000 cm^{-1}. As discussed in Part 3, the

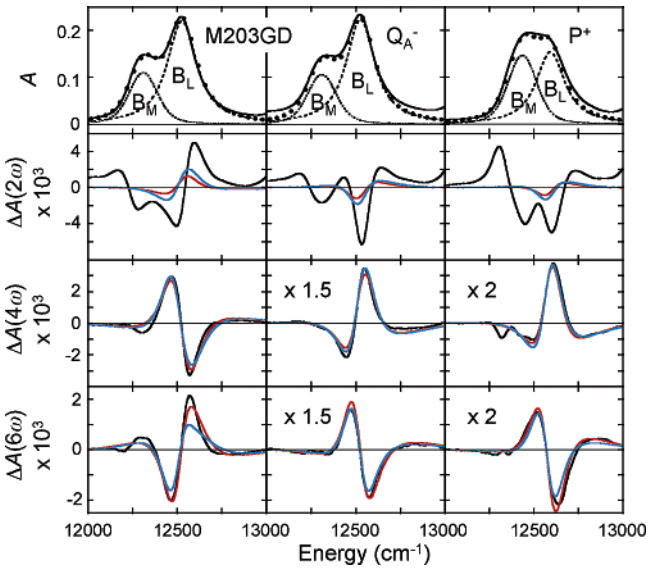

Figure 5. Absorption and Stark fits for M203GD (left), M203GD Q_A^- (middle), and M203GD P^+ (right). In the absorption panels, the data (solid) are plotted with the best fit of the B_L band (dashed), the B_M band (dotted), and their sum (circles). The red spectra in the M203GD Stark panels are the best simultaneous fit to its 4ω and 6ω spectra when δ, W_R, and $f\Delta\mu_R$ are varied; red spectra for the other variants are determined by optimizing the value of δ given the values of W_R and $f\Delta\mu_R$ determined for M203GD. The blue spectra in the M203GD Q_A^- Stark panels are the best simultaneous fit to its 4ω and 6ω spectra when δ, W_R, and $f\Delta\mu_R$ varied; blue spectra for the other variants are determined by optimizing the value of δ given the values of W_R and $f\Delta\mu_R$ determined for M203GD Q_A^-. See Table 1 for best fit values when δ, W_R, and $f\Delta\mu_R$ are simultaneously optimized for each variant.

Lorentzian and Gaussian contributions to the B_M and B_L line shapes arise from homogeneous and inhomogeneous broadening mechanisms, respectively, and enter the calculation of resonance Stark effects differently. As highlighted by the fits to the individual bands using $\Gamma_0 = 90\ cm^{-1}$ and $\Gamma_{Gaus} = 50\ cm^{-1}$ for B_L, and $\Gamma_0 = 35\ cm^{-1}$ and $\Gamma_{Gaus} = 150\ cm^{-1}$ for B_M, the higher energy band in M203GD is both broader at its base and narrower at its peak than the lower energy band. For the case of WT Q_A^- RCs at 85 K, the lifetimes of B_L^* and B_M^*, τ, are 160 fs, as measured both by the rise in fluorescence from P* following excitation of either B_L or B_M or from the fluorescence from B*;[10,12] assuming that the lifetimes of B_L^* and B_M^* in M203GD RCs do not deviate substantially from this value (lifetimes of B* have not been measured by fluorescence from M203GD samples), we estimate the contribution of lifetime broadening to the value of Γ_0 in M203GD RCs as $(2\pi c\tau)^{-1} = 35\ cm^{-1}$, where c is the speed of light. Since this value is the same as that we have used to fit the absorption of B_M, it suggests that the lifetime of B_M^* is the principal component to its homogeneous line width; on the other hand, the greater homogeneous line width of the B_L band suggests that it has a more significant contribution from dephasing. Analyses of time-resolved nonlinear optical measurements by Fleming and co-workers support this interpretation.[34] The greater narrowness at the peak of the B_L band suggests less inhomogeneity in the structure of the B_L binding site compared to that of B_M. This is consistent with the considerably smaller temperature factors that have been determined for B_L by X-ray diffraction.[35]

The ratio of the integrated intensities of the B_L and B_M bands in this fit is 2.5:1. This ratio is not close to 1:1, suggesting the presence of electronic interactions such as the one discussed above between the chromophores in the B_L and H_L binding sites in M214LH RCs. The different intensities of the B_M and B_L bands can be explained either by substantial differences in the excitonic interactions on the M and L branches of the RC or by substantial mixing of the B_M and B_L transitions with each other, for example, mediated by their excitonic interactions with P (see below).[27,29] This deviation is too large to be explained by the small absorption by P in this region or the small vibronic broadening of the B_M and B_L bands characterized above.

Given a description of the B band of M203GD and the experimental values of F and χ used for this sample, five other parameters remain for characterizing the resonance Stark effects of B_L: Δ_{CT}, δ, W_R, $f\Delta\mu_R$, and ζ_{CT}. The value of ζ_{CT} can be determined independently of the other four from the ratios of either the 4ω or 6ω spectra acquired at $\chi = 90°$ and $\chi \neq 90°$. For most of the 12 samples in this study, the exceptions being WT Q_A^- and WT P^+, the two values of ζ_{CT} thus determined were generally within a few degrees of each other and 45°, so we set the value of ζ_{CT} to 45° for fitting the Stark spectra of M203GD.[37] It is interesting to note that this value is close to the value of 54° that is calculated from the structure of WT RCs assuming that the $B_L^* \leftarrow B_L$ transition lies along the line containing nitrogen atoms 1 and 3 of B_L and that the charge transfer takes place between the centers of B_L and H_L;[35] the 45° value is also very different from the value of ζ found for the classical Stark effect of isolated BChl *a* in an organic matrix.[31]

To determine the values of Δ_{CT}, δ, W_R, and $f\Delta\mu_R$ for M203GD, we assume a preliminary value of $1000\ cm^{-1}$ for Δ_{CT} and minimize the sum of the squared residuals from simultaneous comparisons of the calculated line shapes and amplitudes to observed 4ω and 6ω spectra.[38] In this case, the fit values of the Δ_{CT}-reduced variables δ, W_R, and $f\Delta\mu_R$ are -0.34, $1.3\ cm^{-1}$, and 1.06 cm/MV, respectively. Stark spectra calculated using these values (red) are plotted with the observed M203GD Stark spectra (black) in the left panels of Figure 5. The simultaneous fit to the 4ω and 6ω spectra is quite good, with close agreement between the calculation and the data over most of the plotted region. The value of k_{et} for $B_L^* \rightarrow B_L^+H_L^-$ from this fit is 2.0 ps and will be discussed in more detail below. Assuming $\Delta_{CT} = 1000\ cm^{-1}$, the values of fd_{CT}, $\bar{\nu}_0 - \bar{\nu}_{CT}$, and V_0 from this fit are equal to 13.1 Å, $-340\ cm^{-1}$, and $36\ cm^{-1}$, respectively, where d_{CT} is the effective distance of charge transfer. Since the value of f is thought to range between 1.0 and 1.3,[23,39] the 13.1 Å value for fd_{CT} lies well within its expected range of values based on these estimates for f and the 11 Å distance between the centers of B_L and H_L in WT RCs.[35] This result justifies using $1000\ cm^{-1}$ for Δ_{CT}.[40] The fit values of $\bar{\nu}_0 - \bar{\nu}_{CT}$ and V_0 will be discussed in greater detail below.

Having established a procedure for fitting resonance Stark spectra, we need only adapt it slightly for the other samples in this study. Since the resolution of the B_M and B_L bands is worse for these other samples, with the exception of M203GD Q_A^-, in each case we simplify the fitting of the B band absorption by using the same values of Γ_0 and Γ_{Gaus} as those determined for the B_M and B_L bands of M203GD. Although we might also use the same ratio of the integrated intensities of these bands, allowing only their total intensities and peak positions to change between samples, as described above it is clear that this ratio has changed significantly from WT to M203GD P^+. Since we find the ratio of 2.5:1 to provide a satisfactory fit to the B band region for both M203GD and WT, we conclude that P-oxidation is the principal source of variation in this ratio from WT to M203GD P^+. We have found 1.3:1 to provide the best fit to the B band region for M203GD P^+ and have used this ratio for fitting the absorption spectra of all the P^+ samples. Because this ratio is both quite different from the ratio of 2.5:1 observed for P-containing RCs and much closer to the ratio of 1:1 expected in the absence of all excitonic interactions, these fits suggest a substantial excitonic interaction between P and either B_M or B_L. Since it is found that P-oxidation increases and decreases, respectively, the heights of B_M and B_L relative to the H band (see Table 1) to a larger extent than can be explained by changes in the H band or by error, we suggest that P mediates a substantial mixing of the B_M and B_L transitions in P-containing RCs.[27,29] Using the two ratios as described, we determined the fit values of δ, W_R, and $f\Delta\mu_R$ for WT and for unmodified, Q_A^-, and P^+ preparations of M203GD, M210YF, and M210YW using $\Delta_{CT} = 1000\ cm^{-1}$. These fit values, as well as the corresponding values of k_{et}, $\bar{\nu}_0 - \bar{\nu}_{CT}$, V_0, and fd_{CT}, are tabulated in Table 1. In each case, the fit value of fd_{CT} justifies the use of $1000\ cm^{-1}$ as a good approximation to the true value of Δ_{CT}. WT Q_A^- and WT P^+ could not be fit satisfactorily, even when the overlapping classical 4ω Stark effects were taken into account.

These values are uncertain to an extent that depends on the uncertainties in the description of the B_L absorption band, the uncertainty in the measured value of ζ_{CT}, the uncertainty in the value of Δ_{CT}, as well as the observed sample-to-sample variation in the spectra, the functional form of $\rho_{FC}(\bar{\nu})$, and the quality of the fit, as judged by the sum of the residuals between the data and the best fit. Tables 2 and 3 summarize the results of propagating sample uncertainties into the fit values of δ, W_R, and $f\Delta\mu_R$ for M203GD and M203GD Q_A^-, respectively. Whereas the results in Table 2 are representative of M203GD, M210YF, and M210YW, each with values of δ closer to zero, the results in Table 3 are representative of the other samples, each with values of δ closer to -1.0. In addition to these

TABLE 1: Summary of Values Used to Fit Absorption and Stark Data in the B Band Region of Wild-type and Mutant *Rb. sphaeroides* Reaction Centers[a]

		absorption fit parameters				other parameters determined prior to Stark fit		reduced resonance Stark parameters and k_{et}				resonance Stark parameters assuming $\Delta_{CT} = 1000$ cm^{-1}		
		B_L		B_M										
	sample	$\bar{\nu}_0$ (cm^{-1})	peak height	$\bar{\nu}_0$ (cm^{-1})	peak height	F (MV/cm)	ζ_{CT} (deg)	δ	W_R (cm^{-1})	$f\Delta\mu_R$ (cm/MV)	k_{et} (ps^{-1})	$\bar{\nu}_0 - \bar{\nu}_{CT}$ (cm^{-1})	V_0 (cm^{-1})	d_{CT} (Å/f)
1	WT	12 470	0.212	12320	0.106	0.71	45	−0.84	3.5	0.77	0.22	−840	59	9.5
2	M203GD	12 530	0.220	12310	0.110	0.67	45	−0.34	1.3	1.06	0.50	−340	36	13.1
3	M203GD Q_A^-	12 530	0.220	12310	0.110	0.64	45	−0.88	2.7	0.88	0.13	−880	52	10.9
4	M203GD P^+	12 595	0.154	12435	0.147	0.64	45	−0.80	1.4	1.04	0.11	−800	37	12.9
5	M210YF	12 445	0.220	12340	0.110	0.70	45	−0.25	1.2	0.95	0.53	−250	35	11.8
6	M210YF Q_A^-	12 430	0.240	12350	0.120	0.67	45	−0.80	2.0	0.91	0.15	−800	45	11.3
7	M210YF P^+	12 470	0.124	12450	0.118	0.63	45	−0.76	3.3	0.83	0.30	−760	57	10.3
8	M210YW	12 435	0.220	12340	0.110	0.67	45	−0.14	0.82	1.04	0.42	−140	29	12.9
9	M210YW Q_A^-	12 410	0.198	12350	0.099	0.68	45	−0.86	1.6	0.93	0.09	−860	40	11.5
10	M210YW P^+	12 470	0.132	12460	0.126	0.79	45	−0.76	2.4	0.86	0.22	−760	49	10.7

[a] All fits to resonance stark effects of the B_L bands were determined using $\Gamma_0 = 90$ cm^{-1} and $\Gamma_{Gaus} = 50$ cm^{-1}.

TABLE 2: Sensitivity Analysis for M203GD[a]

alteration to fit	change in fit values: δ	W_R (cm^{-1})	$f\Delta\mu_R$ (cm/MV)	sum of squared residuals
$\bar{\nu}_0 + 20$ cm^{-1}	+0.08	+0.1	−0.02	43
$\bar{\nu}_0 - 20$ cm^{-1}	−0.07	−0.1	+0.02	29
peak height + 20%		−0.1	−0.02	25
peak height − 20%		+0.2	+0.03	27
$2\Gamma_0 + 20\%$ of $(2\Gamma_0 + \Gamma_{Gaus})$		−0.1	+0.03	63
$2\Gamma_0 - 20\%$ of $(2\Gamma_0 + \Gamma_{Gaus})$		+0.1	−0.04	13
$\Gamma_{Gaus} + 20\%$ of $(2\Gamma_0 + \Gamma_{Gaus})$		−0.1	+0.03	67
$\Gamma_{Gaus} - 20\%$ of $(2\Gamma_0 + \Gamma_{Gaus})$		−	−0.02	17
$\zeta_{CT} + 10°$		−0.1	−0.03	22
$\zeta_{CT} - 10°$		+0.1	+0.04	33
$\Delta_{CT} + 50\%$	+0.01	−0.2	+0.03	50[b]
$\Delta_{CT} - 50\%$	+0.01	+0.4	−0.04	34[c]
$4\omega \times 1.4$, $6\omega \times 1.7$			+0.11	26[d]
$4\omega/1.4$, $6\omega/1.7$			−0.10	26[e]
$G(\bar{\nu})$ instead of $P(\bar{\nu})$	+0.02		+0.03	35

[a] When 250 evenly spaced points within ±500 cm^{-1} of $\bar{\nu}_0$ were used, the fit to this mutant yielded $\delta = -0.34$, $W_R = 1.3$ cm^{-1}, $f\Delta\mu_R = 1.06$ cm/MV, and a sum of squared residuals equal to 26. The changes to this sum and the fit values of δ, W_R, and $f\Delta\mu_R$ are tabulated as a function of the alterations to either the fit procedure or the data described in the left-hand column. [b] Since 167 points were used for this calculation, the resulting sum of squared residuals has been multiplied by 1.5 for better comparison. [c] Since 500 points were used for this calculation, the resulting sum of squared residuals has been divided by 2 for better comparison. [d] Because the residuals increase linearly with the size of the spectrum, we have divided the sum of the squared residuals in this case by the average of $(1.4)^2$ and $(1.7)^2$ for better comparison. [e] Because the residuals decrease linearly with the size of the spectrum, we have multiplied the sum of the squared residuals in this case by the average of $(1.4)^2$ and $(1.7)^2$ for better comparison.

TABLE 3: Sensitivity Analysis for M203GD Q_A^-[a]

alteration to fit	change in fit values: δ	W_R (cm^{-1})	$f\Delta\mu_R$ (cm/MV)	sum of squared residuals
$\bar{\nu}_0 + 20$ cm^{-1}	+0.02	+5.8	−0.23	9.9
$\bar{\nu}_0 - 20$ cm^{-1}	−0.07	−0.6	+0.08	4.9
peak height + 20%	−	−0.3	−0.02	5.5
peak height − 20%	−0.02	+1.1	−0.02	4.2
$2\Gamma_0 + 20\%$ of $(2\Gamma_0 + \Gamma_{Gaus})$		+1.1	−0.06	13
$2\Gamma_0 - 20\%$ of $(2\Gamma_0 + \Gamma_{Gaus})$		−0.8	+0.04	6.4
$\Gamma_{Gaus} + 20\%$ of $(2\Gamma_0 + \Gamma_{Gaus})$	−0.02	+2.0	−0.09	15
$\Gamma_{Gaus} - 20\%$ of $(2\Gamma_0 + \Gamma_{Gaus})$		−0.6	+0.04	4.4
$\zeta_{CT} + 10°$		−0.1	−0.03	5.1
$\zeta_{CT} - 10°$		+0.2	+0.03	4.6
$\Delta_{CT} + 50\%$	+0.01	−0.2		7.6[b]
$\Delta_{CT} - 50\%$	−0.04	+3.7	−0.16	28[c]
$4\omega \times 1.4$, $6\omega \times 1.7$	−0.02	+0.4	+0.07	5.0[d]
$4\omega/1.4$, $6\omega/1.7$		+0.2	−0.10	5.3[e]
$G(\bar{\nu})$ instead of $P(\bar{\nu})$	−0.02	+0.3	+0.03	6.3

[a] When 250 evenly spaced points within ±500 cm^{-1} of $\bar{\nu}_0$ were used, the fit to this mutant yielded $\delta = -0.88$, $W_R = 2.7$ cm^{-1}, $f\Delta\mu_R = 0.88$ cm/MV, and a sum of squared residuals equal to 4.8. The changes to the fit values of δ, W_R and $f\Delta\mu_R$ are tabulated as a function of the alterations to either the fit procedure or the data described in the left-hand column. [b] Since 167 points were used for this calculation, the resulting sum of squared residuals has been multiplied by 1.5 for better comparison. [c] Since 500 points were used for this calculation, the resulting sum of squared residuals has been divided by 2 for better comparison. [d] Because the residuals increase linearly with the size of the spectrum, we have divided the sum of the squared residuals in this case by the average of $(1.4)^2$ and $(1.7)^2$ for better comparison. [e] Because the residuals decrease linearly with the size of the spectrum, we have multiplied the sum of the squared residuals in this case by the average of $(1.4)^2$ and $(1.7)^2$ for better comparison.

uncertainties, the values in Table 1 may contain errors from imposing an idealized model upon a real system. Of particular relevance here is the assumption of the resonance Stark theory, made explicit in Part 3, that there is zero vibronic coupling between the ground and excited states of B_L. Indeed this vibronic coupling is small, as indicated by the apparently small Gaussian broadening of the largely symmetric B_L band and by the relatively small intensities of absorption in and immediately above the region dominated by BPhe absorption. These observations indicate that this vibronic coupling is small for specifically low- and high-frequency modes, respectively. Considering also the small Stokes' shift measured for fluorescence from B_L,[12] the total vibronic coupling of the electronic transition to B_L^* must be small such that errors introduced from using this idealized model to fit its HOS spectra should also be small.

Although Tables 2 and 3 demonstrate that a 20 cm^{-1} change in the value of $\bar{\nu}_0$ can yield a change in the fit value of δ of nearly 0.1, they also demonstrate that the quality of the fit is generally so sensitive to the value of $\bar{\nu}_0$ that one can use the Stark spectra to improve an initial estimate of $\bar{\nu}_0$ in cases where there is poor resolution between the B_M and B_L bands. In three out of ten cases (M210YF P^+, M210YW Q_A^-, and M210YW P^+), we found that our attempt to identify the value of $\bar{\nu}_0$ from the absorption spectrum alone benefited significantly from such a correction. In these cases, we have reported the improved value of $\bar{\nu}_0$ and the corresponding fit values.

Discussion

Perturbations to $\bar{\nu}_{CT}$. The fit values of δ in Table 1 give 0.50, 0.59, and 0.70 as the reduced stabilization of $B_L^+H_L^-$ conferred by the M203GD, M210YF, and M210YW mutations, respectively. The reduced destabilization of $B_L^+H_L^-$ by Q_A-reduction is 0.54, 0.55, and 0.72 in the three mutants, respec-

tively. The reduced destabilization of $B_L^+H_L^-$ by P-oxidation is 0.46, 0.51, and 0.62 in the three mutants, respectively. Based on the information in Tables 2 and 3, the uncertainties in these pairwise differences are estimated as 0.10.

Assuming that the value of Δ_{CT} is the same for all preparations,[41] it is noteworthy that the destabilization due to Q_A-reduction is consistently greater than that due to P-oxidation, despite the fact that P is closer to B_L than Q_A is to H_L.[35] The difference between the values of the two destabilization energies is even increased slightly when one takes into account the larger values of $\bar{\nu}_0$ for P-oxidized RCs compared to Q_A-reduced RCs. This implies that the dielectric screening of the charge on Q_A^- is less than the screening of the charge on P^+.[42] This qualitative conclusion implies that P occupies a more polar part of the protein than the deeply buried Q_A.

The effective dielectric screening in the regions around either P^+ or Q_A^- and the probe $B_L^+H_L^-$ can be calculated using crystallographic coordinates and a value for Δ_{CT}. The 14 Å distance between the centers of Q_A and H_L and the 24 Å distance between the centers of Q_A and B_L yield an expected destabilization of $B_L^+H_L^-$ by Q_A equal to 3900 cm^{-1}/ϵ, where ϵ is the effective dielectric screening. Given the 11 Å distance between the centers of P and B_L and the 18 Å distance between the centers of P and H_L, the expected destabilization of $B_L^+H_L^-$ due to P-oxidation is 5700 cm^{-1}/ϵ; this value reduces to 5200 cm^{-1}/ϵ when the asymmetric distribution of the hole on the two halves of P is taken into account.[43] When the value of 1000 cm^{-1} is used for Δ_{CT} for each preparation, as justified above, the average destabilization of $B_L^+H_L^-$ due to Q_A-reduction in the three mutants is 600 cm^{-1}, yielding an estimate for the dielectric screening in the region of the protein around Q_A^- and $B_L^+H_L^-$ equal to 6.5; the average destabilization due to P-oxidation is thus 530 cm^{-1}, yielding an estimate for the dielectric screening in the region of the protein around P^+ and $B_L^+H_L^-$ equal to 9.8. These values, although larger than is often assumed for the interior of a protein when the details of its nuclear configurational reorganization are unknown,[44] are consistent with other estimates that have been made for reaction center proteins. In particular, we note the similarities between these values and those estimated using the absorption and 2ω Stark spectra of WT, WT P^+, and WT Q_A^- at 1.5 K.[25]

Using the value $\Delta_{CT} = 1000$ cm^{-1}, we determined the M203GD, M210YF, and M210YW mutations to stabilize $B_L^+H_L^-$ by 500, 590, and 700 cm^{-1}, respectively. If the charge distribution of the hole on B_L^+ in $B_L^+H_L^-$ is similar to that of the unpaired electron on B_L^- in $P^+B_L^-$, then these same values can be used to quantify the destabilization of $P^+B_L^-$, which has been invoked as a contribution to a slowing of the primary charge-separation process $P^* \rightarrow P^+B_L^-$ in these mutants compared to WT.[20,21,45] To make this estimate, these values must be corrected for the possibly significant effect of these mutations on the energy of P^+. These perturbations can be estimated by the changes in the P/P^+ oxidation potential due to these mutations with the caveat that these changes, measured at room temperature, may be largely determined by long time scale reorganizations of the protein around the radical cation that would not occur upon formation of the short-lived $P^+B_L^-$:[20,21] they are 0, 260, and 430 cm^{-1} for M203GD, M210YF, and M210YW, respectively. Thus we estimate the increases in the energy of $P^+B_L^-$ relative to the energy of P* as 500, 850, and 1130 cm^{-1}, respectively. This ordering of the mutations by increasing energy of $P^+B_L^-$ relative to P* is the same as their ordering by increasing lifetime of P* near room temperature.[20,21]

Perturbations to V_0 and d_{CT}. Table 1 contains several interesting trends in addition to the energies of interaction between charge-transfer states and modifications to the protein, in particular, substantial differences in values for the reduced coupling, W_R. For example, the fit value of W_R is 0.82 cm^{-1} for M210YW but 3.5 cm^{-1} for WT and 1.3 cm^{-1} for M203GD but 2.7 cm^{-1} for M203GD Q_A^-. These differences may be due to differences in the values of V_0 among the variants studied. Although the electronic couplings for charge-transfer reactions are expected to be exquisitely sensitive to even small structural perturbations, as might occur in the RC when mutations are made, P is oxidized, Q_A is reduced, or the temperature is changed, their values are usually assumed to be unaffected by these kinds of perturbations to simplify the interpretation of kinetic data. Because the application of an electric field to a frozen sample should not perturb the structure of a charge-transfer system, resonance Stark effects are preferable to these other methods for determining a value of V_0.

The significance of the variation in W_R documented in Table 1 is supported both by the sensitivity analyses in Tables 2 and 3 and by the failure of the 10 extracted values of W_R to be distributed in a random manner (i.e., the density of these values is not largest about its mean). The comparison between M203GD and M203GD Q_A^- is the most straightforward to make specifically because these samples have nearly identical absorption spectra, these absorption spectra have been well-characterized, and we have reported the sensitivity analyses explicitly for these samples. Whereas the sensitivity analysis for M203GD (Table 2) suggests that its value of W_R is well-determined, the sensitivity analysis for M203GD Q_A^- (Table 3) reveals that uncertainties in some parameters significantly affect the fit value of W_R. Nevertheless, the uncertainties in the fit value of 2.7 cm^{-1} for M203GD Q_A^- are asymmetric, tending to make this value larger and thus tending to increase its difference from the fit value of 1.3 cm^{-1} for M203GD. The only significant uncertainties that act to decrease the fit value of W_R for M203GD Q_A^- arise from decreasing the peak width of the B_L band and shifting it to lower energy. Although it is indeed likely that we have overestimated the width of the B_L band somewhat by attempting to account for all the intensity in the B band region with only two symmetric bands, it is also likely that we have overestimated the peak intensity of this band for the same reason. The uncertainties in the peak intensity and width are thus correlated; since the corresponding uncertainties in the fit value of W_R act in opposing directions, the overall effect of overestimating the peak width is smaller than suggested by Table 3. Although the fit quality of the Stark spectra, as judged by the sum of the squared residuals, is not much affected by the small reduction in the value of $\bar{\nu}_0$, the increased overlap between the B_L and B_M bands that this would engender would also require reducing the peak height of the B_L band. The uncertainties in peak intensity and position are thus correlated as well; since the corresponding uncertainties in the fit value of W_R act in opposing directions, the overall effect of overestimating the peak position is smaller than suggested by Table 3.

The red and blue curves in Figure 5 illustrate the significance of these differences graphically. For each of the Stark spectra, the red curves correspond to the best fit using the values of W_R and $f\Delta\mu_R$ as determined from simultaneously fitting the 4ω and 6ω spectra of M203GD and the blue curves correspond to the best fits using the values of W_R and $f\Delta\mu_R$ as determined from fitting the M203GD Q_A^- spectra. In the case of M203GD, the blue fit to the 6ω spectrum is clearly inferior to the red fit. Taken individually, neither of the red fits to the 4ω or 6ω spectra

of M203GD Q_A^- is as poor as the blue fit to the 6ω spectrum of M203GD, but taken together, the discrepancies in this case are significant. The fact that the red fit to the 4ω spectrum of M203GD Q_A^- is too small while the red fit to its 6ω spectrum is too large cannot be attributed to any reasonable combination of the experimental errors that we have characterized above. For example, modifying the estimated sample thickness to increase the quality of the fit to one spectrum must decrease the quality of the fit to the other.

These differences among the fit values of W_R can be attributed to differences among the values of either V_0 or Δ_{CT}. Although it is unlikely that Δ_{CT} should take significantly different values for different variants of RCs,[41] it is important to note that differences in Δ_{CT} should not account for more than a small fraction of the differences in W_R for two other reasons: first, the fit quality reported in Tables 2 and 3 decreases substantially when the value of Δ_{CT} is altered by 50%; second, any attempt to decrease the dispersion in the fit values of V_0 by varying Δ_{CT} would only increase the range of fit values of d_{CT} (see Table 1). When $\Delta_{CT} = 1000$ cm^{-1} is used for all variants, this range, between 9.5 Å/f for WT and 13.1 Å/f for M203GD, straddles the 11 Å distance between the centers of B_L and H_L that is estimated from the wild-type crystal structure.[35] Although the distance between B_L and H_L does not appear to change much among crystal structures of RC variants, the crystallographic resolution of these structures is rarely better than 2.5 Å. The apparent spread in values may also reflect the influence of factors such as the electronic polarizabilities of B_L^+ and H_L^-, which could make the center-to-center distance an inaccurate estimator of the effective charge-transfer distance, d_{CT}. Interestingly, Stark spectra due to a different charge-transfer process involving bacteriochlorins, those of the mid-infrared intervalence band of P^+ in WT, have been fit with an effective charge-transfer distance that is roughly 20% shorter than the center-to-center distance for this hole transfer.[46] With these issues in mind, the range from 9.5 Å/f to 13.1 Å/f does not seem unreasonable for d_{CT}, especially when one considers that the substitutions of aspartic acid and tryptophan for glycine and tyrosine significantly increase the volume of the side chains at positions M203 and M210, respectively. However, since it seems unlikely that this range could be as large as it would be if the dispersion in the fit values of V_0 were eliminated by allowing Δ_{CT} to vary, we conclude that changes in the fit values of W_R are due, at least partly, to differences in the values of V_0. When $\Delta_{CT} = 1000$ cm^{-1} is used, the fit values of V_0 extend from 29 cm^{-1} for M210YW to 59 cm^{-1} for WT. It is interesting to note that these values, constrained by the crystallographically estimated charge-transfer distance, are each consistent with the range of values of V_0 estimated for either $B_L^* \rightarrow B_L^+H_L^-$ or $P^+B_L^- \rightarrow P^+H_L^-$ from structure-based calculations.[47,49]

On the other hand, it would be unexpected if changes in the fit values of d_{CT} were *not* accompanied by changes in the fit values of V_0 since the electronic coupling is expected to be highly sensitive to structural perturbations. According to the simplest model for the relationship between V_0 and the structure of a charge-transfer system, it is expected that

$$V_0^2 \propto \exp(-\beta d_{ee}) \qquad (1)$$

where d_{ee} is the edge-to-edge distance between B_L and H_L and β is a constant that characterizes the sensitivity of the electronic coupling to d_{ee}. A value of β equal to 1.4 Å^{-1} has been estimated from kinetic measurements of multiple charge-transfer processes in RCs, but quite different values have been obtained in other systems.[50] This value suggests that V_0 is so sensitive to structural perturbation that the largest difference in d_{ee} among the variants need only be 1 Å to account for the range of fit values of V_0; conversely, if the largest difference in d_{CT} in Table 2 is presumed equal to the largest difference in d_{ee} and f is assumed equal to 1.0, then the value of V_0 for $B_L^* \rightarrow B_L^+H_L^-$ is expected to span more than an order of magnitude. Despite the expected sensitivity of V_0 to mutation, there are few examples in the literature where such changes have been clearly identified, much less quantified.[68] Interestingly, the plot of $\ln(V_0^2 \cdot \text{cm}^2)$ (see Figure 6) against d_{CT} in Figure 6 can be fit with a straight line of slope 0.4 f/Å in a manner analogous to eq 1. The difference between this slope and the value of 1.4 Å^{-1} can be explained in large part by recognizing that a change in d_{ee} may be significantly smaller than the corresponding change in d_{CT} for the same structural perturbation; for example, structural perturbations that act to fold B_L in toward H_L will decrease d_{CT} to a larger extent than they decrease d_{ee}. But it is important to note that the previous estimate of β relied on the assumption that values of V_0 for other reactions were unaffected by the same kinds of perturbations that we have shown to affect the value of V_0 for the reaction investigated here. It was reasonable to have made that assumption because any perturbations to the values of V_0 for those reactions could not be characterized using kinetic measurements. In contrast, resonance Stark effects can characterize changes in V_0 as described here. An illustration of how the interpretation of kinetic data might change depending on knowledge of how V_0 changes is presented below.

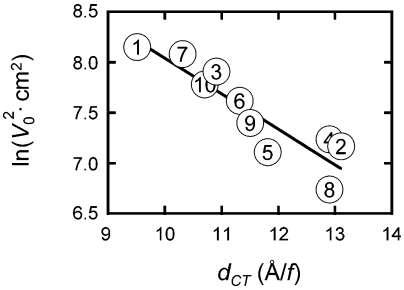

Figure 6. Plot of $\ln(V_0^2 \cdot \text{cm}^2)$ against d_{CT} using values from Table 1. Points are fit to a line with a slope of 0.4 f/Å.

Just as the measurements of stabilization above yielded insight into the primary charge-separation process, $P^* \rightarrow P^+B_L^-$, so do these measurements of charge-transfer distance and electronic coupling. If B_L and H_L are organized to optimize the contribution of electronic coupling to the rate of formation of $P^+H_L^-$ from $P^+B_L^-$, then a likely parallel effect is the optimization of the electronic coupling between B_L^* and $B_L^+H_L^-$ since the same orbitals are occupied by the transferred electron in each process. On the other hand, if the environments of B_L and H_L are organized so as to optimize the rate of $P^+B_L^- \rightarrow P^+H_L^-$ by making it an activationless reaction, $B_L^* \rightarrow B_L^+H_L^-$ need not also be an activationless reaction. Although the reorganization energies for $P^+B_L^- \rightarrow P^+H_L^-$ and $B_L^* \rightarrow B_L^+H_L^-$ are probably similar, since they involve distortions of the same molecules and the same environment to the same changes in charge, the driving forces may be substantially different due to different distributions of charge in the initial and final states of the two reactions. Interestingly, for $B_L^* \rightarrow B_L^+H_L^-$ we find the largest electronic coupling for WT, even though in WT this reaction is further from being activationless than in M203GD, M210YF, or M210YW.

Second, the observation that mutations have greatly perturbed not only the driving force for $B_L^* \rightarrow B_L^+H_L^-$ but also its

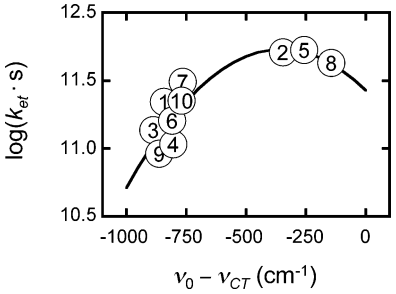

Figure 7. Plot of $\log(k_{et}\cdot s)$ against $\bar{\nu}_0 - \bar{\nu}_{CT}$ using values from Table 1. Points are fit to a parabola.

electronic coupling suggests that mutations that perturb the driving force for either $P^* \rightarrow P^+B_L^-$ or $P^+B_L^- \rightarrow P^+H_L^-$ also perturb the electronic couplings for these reactions. Since plots of rate versus driving force are generally analyzed under the assumption that the electronic coupling is the same for all conditions, the observations here suggest that the values of electronic coupling that have been extracted from these analyses may be inaccurate.[50] This insight could contribute to the discrepancy between the slope of 0.4 *f*/Å in Figure 6 and the 1.4 $Å^{-1}$ value of β estimated previously.

Perturbations to k_{et}. The results in Table 1 include the different rate constants for $B_L^* \rightarrow B_L^+H_L^-$ calculated using eq 38 from Part 3 and the fit values of W_R and δ for each variant. In Figure 7, these values are plotted against $\bar{\nu}_0 - \bar{\nu}_{CT}$. This plot of rate versus driving force resembles plots generated from kinetic measurements and redox potentials of other charge-transfer reactions in RCs.[50,62−65] To provide an example of how the reorganization energies and electronic couplings determined from such plots can be mistaken, the points in Figure 7 are fit to a parabola under the assumption that a single value of V_0 applies to all points (see eq 2 below). This fit misidentifies the value of the reorganization energy by 350 cm^{-1} since it peaks at 350 cm^{-1} below the energy where the driving force is truly equal to the reorganization energy ($\bar{\nu}_0 - \bar{\nu}_{CT} = 0$ cm^{-1}). The fit also yields a value of 20 cm^{-1} for V_0, which is only $^1/_3$ its value for WT since the fit value is most strongly influenced by the electronic couplings of the variants that are closest to the peak of the fit.

Although much work has been done in the time domain to characterize the excited-state dynamics in RCs following excitation of B_L,[2,10−18] there has been no unambiguous measurement of the rate of $B_L^* \rightarrow B_L^+H_L^-$ in either WT or mutant RCs. Whereas the 160 fs lifetime of B_L^* at 77 K has been measured with high precision in WT Q_A^- using the fluorescence upconversion gating technique,[10] attempts to determine by other methods the quantum yields of the products of B_L^* decay have caused much confusion. For example, Woodbury and co-workers,[15] Martin and co-workers,[14] and van Grondelle and co-workers[18] have each measured ultrafast transient absorption spectra of WT RCs (Q_A^-, Q-depleted, and unmodified samples, respectively). Each has noted excitation wavelength-dependent kinetics across the Q_y region, which are inconsistent with the simple reaction scheme $B_L^* \rightarrow P^* \rightarrow P^+H_L^-$, and each has considered the possibility of direct charge transfer from B_L^* in interpreting their results; however, each has arrived at a different conclusion. Whereas van Grondelle and co-workers conclude that 60% of B_L^* transfers its energy to P and the remaining 40% forms $P^+B_L^-$, Martin and co-workers conclude that 50% of B_L^* transfers its energy to P and the remaining 50% forms $B_L^+H_L^-$. It is difficult to imagine that the differences in sample preparation or pump and probe pulse widths or other experimental conditions for these two fundamentally similar experiments would yield RC populations with similar efficiencies of energy transfer at the same time that they undergo different charge-transfer reactions. The differences between the data of the two groups are perhaps better explained by the interpretation Woodbury and co-workers have put forth for the data from a third, also similar experiment: they propose that much of the excitation wavelength-dependent kinetics is not due to any kind of direct charge transfer from B_L^* but rather is due to heterogeneity in the reaction center population.

This third conclusion is also the most consistent with the results of the present study. Martin and co-workers conclude that $B_L^* \rightarrow B_L^+H_L^-$ occurs with a rate equal to $^1/_2$ of $(160\ fs)^{-1}$; this rate is too fast to be consistent with the values of electronic coupling that we have determined (see below). Although the slower rate that van Grondelle and co-workers have proposed for this reaction is more consistent, their claim that $P^+B_L^-$ is formed directly from B_L^* would appear to be inconsistent with our results. Since Q_A-reduction is unlikely to have a substantial effect on the energy of $P^+B_L^-$, the ultrafast hole transfer from B_L^* to P that van Grondelle and co-workers have reported for unmodified WT RCs ought to exhibit a large signal at B_L in the Stark spectrum of WT Q_A^- RCs. Since this signal is not observed, we find that it is unlikely that $P^+B_L^-$ could form by an ultrafast incoherent process in unmodified WT RCs. Although one might reserve judgment on the accuracy of our quantitative results until we have been able to make some direct comparisons between rates measured in the time domain and rates calculated from fitting resonance Stark spectra,[51] the physical principles underlying the resonance Stark effect are the same as those used generally to understand both the kinetic and spectroscopic manifestations of all radiationless transitions, including charge-transfer reactions. In this context, one expects an ultrafast, incoherent charge transfer over a distance of roughly 10 Å to be accompanied by a sizable resonance Stark effect, which reflects the perturbation by the electric field to the excited-state lifetime of the transition. That no such Stark effect is observed in WT Q_A^- RCs is most consistent with the interpretation of transient absorption data by Woodbury and co-workers.

Of the mutants in this study, only M210YW has received similar scrutiny by transient absorption spectroscopy. van Grondelle and co-workers have concluded that 43% of B_L^* undergoes direct charge transfer to form $P^+B_L^-$ and $B_L^+H_L^-$ with a 2:1 ratio of quantum yield.[16] Their identification of $P^+B_L^-$ as a direct product of B_L^* excitation is inconsistent with the results of this study for the same reasons as described above.

Fluorescence excitation spectra have also been used to characterize the quantum yield of energy transfer from B_L^* to P. When the fluorescence excitation spectrum of R26 RCs by Lutz and co-workers[52] is compared with that by Michel-Beyerle and co-workers,[53] the differences among the relative heights of the Q_y bands in these spectra reflect the difficulty of this experiment. Despite the differences in the experimental results, both groups conclude that the fluorescence excitation spectra resemble the absorption spectra of R26 RCs, implying that some differences between absorption spectra and fluorescence excitation spectra do not provide conclusive evidence that the quantum yield of energy transfer from B_L^* to P is significantly less than 1. The larger differences between the fluorescence excitation spectra of M210YW RCs by Hoff and co-workers[54] and by van Grondelle and co-workers[55] again reflect the difficulty of this experiment. However, whereas Hoff and co-workers conclude that B_L^* transfers its energy efficiently to P, van Grondelle and

co-workers conclude that the quantum yield for $B_L^* \rightarrow P$ is only about 60%. The same group has used fluorescence excitation spectra to conclude that the quantum yield for $B_L^* \rightarrow P$ in M210YF is also about 60%, increasing to about 75% in Q_A^- samples of both mutants.[56]

This increase in the quantum yield of $B_L^* \rightarrow P$ upon Q_A-reduction is consistent with our measurements of the decreased rate of $B_L^* \rightarrow B_L^+H_L^-$ upon Q_A-reduction; however, the values of the quantum yields that van Grondelle et al. have reported appear inconsistent with the lifetimes reported in Table 1. Using the 160 fs lifetime that has been determined for B_L^* in WT Q_A^- RCs by the fluorescence upconversion gating technique and the roughly $(2.0\ ps)^{-1}$ rates of electron transfer that we have determined for unmodified M210YF and M210YW samples from the analysis of resonance Stark spectra, we would predict smaller quantum yields of $B_L^+H_L^-$ in these samples (roughly 10%). However, these results may be more consistent than this comparison suggests if strong interactions with the thermal bath following the excitation of B_L were to boost the reaction rate compared to what we have determined from fitting resonance Stark effects, which is a rate of tunneling from the ground vibrational state of B_L^*.

In the limit where the dominant mechanism of charge transfer is thermal activation, this rate is given by

$$k_{et}(T) = \frac{2|V_0|^2}{h}\sqrt{\frac{\pi^3}{\lambda k_B T}}\exp\left[\frac{-(\Delta\bar{\nu}+\lambda)^2}{4\lambda k_B T}\right] \qquad (2)$$

where h is Planck's constant and k_B is Boltzmann's constant.[57] This limit is not likely to be applicable for $B_L^* \rightarrow B_L^+H_L^-$ at 77 K, but it provides a simple estimate of a possible rate enhancement from thermal energy. To calculate this rate from the fit to a resonance Stark effect, one needs to determine the reorganization energy, λ, and driving force, $\Delta\bar{\nu}$. Given the 1000 cm^{-1} estimate for Δ_{CT} and the fit values of δ for these variants, these energies can be calculated using eqs 42 and 43 in Part 3; the only other quantity that is needed is $\bar{\nu}_{mean}$, the mean vibrational frequency of the modes that are coupled to this charge-transfer reaction.

Previous estimates of $\bar{\nu}_{mean}$ for charge-transfer processes in RCs range widely. For example, Reimers and Hush have estimated the value of $\bar{\nu}_{mean}$ for the hole transfer between the two halves of P^+ as 1200 cm^{-1};[58] Treynor et al. find that 650 cm^{-1} gives a better fit to the Stark spectrum of the intervalence band of P^+;[46] Bixon and Jortner have suggested a value of 100 cm^{-1} for electron-transfer processes involving Q_A.[59] A combination of high and low frequency modes has also been used to describe some processes. At 77 K, if $\bar{\nu}_{mean}$ equals either 100 or 650 cm^{-1}, eq 2 yields a rate of activated electron transfer for M210YF that is 0.9 ps, twice as fast as its tunneling rate from the ground vibrational state of B_L^*; the quantum yield for $B_L^+H_L^-$ formation is thus roughly 25%, using the 160 fs lifetime for B_L^*, which is more consistent with the value of 40% estimated by van Grondelle and co-workers from transient absorption spectra. The rate of activated electron transfer for M210YW in these cases is either 1.2 or 0.6 ps, respectively; in the latter case, the quantum yield is roughly 35%. However, the value of 650 cm^{-1} for $\bar{\nu}_{mean}$ leads to $B_L^+H_L^-$ being higher in energy than B_L^* by almost 600 cm^{-1} for WT RCs. This situation is highly unlikely since there could be no significant tunneling (or resonance Stark effect) without satisfying the resonance condition between the ground vibrational state of B_L^* and the vibrational states of $B_L^+H_L^-$. Thus it appears difficult to reconcile the rates determined here by analyses of resonance Stark effects with those assigned to these processes by various fits of transient absorption changes.

Because the theory of resonance Stark effects has been developed for a resonant tunneling process, one does not expect the equations and spectra developed in Parts 2 and 3 to accurately describe the Stark spectra of a complex for which its charge-transfer state is out of resonance with its excited state for a large portion of a sample. This expectation can be used to provide a rough estimate of the value of $\bar{\nu}_{mean}$ for $B_L^* \rightarrow B_L^+H_L^-$ from the Stark spectra of WT Q_A^- and WT P^+, the two variants for which Stark spectra could not be fit well with the theory of resonance Stark effects. For example, a value of 150 cm^{-1} makes $B_L^+H_L^-$ lower in energy than B_L^* by 360 cm^{-1} for WT. Since we have determined Q_A-reduction and P-oxidation to destabilize the formation of $B_L^+H_L^-$ by 600 and 530 cm^{-1}, respectively, the value of 360 cm^{-1} for $\Delta\bar{\nu}$ in WT implies that the Stark spectra of B_L for WT Q_A^- and WT P^+ should not behave according to the theory of resonance Stark effects that we have developed. As the estimate of $\bar{\nu}_{mean}$ decreases, the energy of $B_L^+H_L^-$ decreases with respect to the energy of B_L^*, so the discrepancy between experiment and theory for WT Q_A^- and WT P^+ becomes more difficult to explain; conversely, as the estimate of $\bar{\nu}_{mean}$ increases, the energy of $B_L^+H_L^-$ increases with respect to B_L^* such that the close agreement between experiment and theory for the Stark spectra of WT and other variants becomes more difficult to explain. Lending additional support to this rough estimate of 150 cm^{-1} for $\bar{\nu}_{mean}$ is the corresponding value for the reorganization energy, 1200 cm^{-1}; this value is similar to that which has been estimated for the charge transfer between the two bacteriochlorins that make up the oxidized special pair.[46,58]

Conclusions

This investigation into the factors that control the rate of $B_L^* \rightarrow B_L^+H_L^-$ has yielded quantitative estimates for the perturbations to the charge-transfer distance, d_{CT}, and electronic coupling, V_0, that accompany perturbations to the driving force for this reaction. Using the crystallographic estimate of 11 Å between the centers of B_L and H_L in WT RCs as a preliminary estimate for d_{CT}, we have estimated the value of the full width at half-maximum of the Franck−Condon weighted density of states, Δ_{CT}, to be 1000 cm^{-1}. Having argued that Δ_{CT} is least likely among these other parameters to take different values in the different reaction center variants studied, we have found the values of d_{CT} for these variants to range by as much as 1.5 Å above and below their mean value of 11.5 Å. Using $\Delta_{CT} =$ 1000 cm^{-1}, we have found the largest and smallest values of V_0 for these variants to range between 30 and 60 cm^{-1} and the mean perturbations to the energy of $B_L^+H_L^-$ by Q_A-reduction and P-oxidation to be 600 and 530 cm^{-1}, respectively. Using crystallographic estimates of distance, we have found the dielectric screening of the charges on Q_A and P to be 6.5 and 9.8, respectively, in the regions containing either Q_A or P and the probe $B_L^+H_L^-$. We have also argued that resonance Stark effects are capable of yielding a quantitative estimate of 150 cm^{-1} for the mean vibrational frequency of the modes that are coupled to the $B_L^* \rightarrow B_L^+H_L^-$ charge-transfer reaction. To reduce the uncertainties in each of these results, it was necessary to characterize and avoid artifacts in data acquisition and data analysis. This process depends critically on the analysis of the absorption spectrum of the Q_y region of RCs; further improvements in this analysis will improve the results from the resonance Stark analysis. Increasing the spectral resolution by

making mutants in the M203GD background, by displacing the B_M chromophore altogether, or by using lower temperature should provide better characterization of the issues approached here.

Acknowledgment. T.P.T. is supported by a predoctoral fellowship from the Fannie and John Hertz Foundation and a Stanford Graduate Fellowship. C.Y.-I. is supported by a postgraduate fellowship from the Natural Sciences and Engineering Research Council of Canada and a Gabilan Stanford Graduate Fellowship. This work was supported by the NSF Biophysics and Chemistry Programs. We thank Dr. Brett A. King for useful discussions.

References and Notes

(1) *The Photosynthetic Reaction Center*; Deisenhofer, J., Norris, J. R., Eds.; Academic Press: San Diego, CA, 1993.

(2) Woodbury, N. W.; Becker, M.; Middendorf, D.; Parson, W. W. *Biochemistry* **1985**, *24*, 7516. Breton, J.; Martin, J.-L.; Migus, A.; Antonetti, A.; Orszag, A. *Proc. Natl. Acad. Sci. U.S.A.* **1986**, *83*, 5121.

(3) Kirmaier, C.; Holten, D. *Photosynth. Res.* **1987**, *13*, 225.

(4) Joseph, J.; Bruno, W.; Bialek, W. *J. Phys. Chem.* **1991**, *95*, 5.

(5) Zhou, H. L.; Boxer, S. G. *J. Phys. Chem. B* **1998**, *102*, 9139.

(6) Zhou, H. L.; Boxer, S. G. *J. Phys. Chem. B* **1998**, *102*, 9148.

(7) Treynor, T. P.; Boxer, S. G. *J. Phys. Chem. B* **2004**, *108*, 13513.

(8) Robinson, G. W.; Frosch, R. P. *J. Chem. Phys.* **1962**, *37*, 1962.

(9) Markham, J. J. *Rev. Mod. Phys.* **1959**, *31*, 956.

(10) Stanley, R. J.; King, B. A.; Boxer, S. G. *J. Phys. Chem.* **1996**, *100*, 12052.

(11) King, B. A.; Stanley, R. J.; Boxer, S. G. *J. Phys. Chem. B* **1997**, *101*, 3644.

(12) King, B. A.; McAnaney, T. B.; deWinter, A.; Boxer, S. G. *J. Phys. Chem. B* **2000**, *104*, 8895.

(13) King, B. A.; deWinter, A.; McAnaney, T. B.; Boxer, S. G. *J. Phys. Chem. B* **2001**, *105*, 1856.

(14) Vos, M. H.; Breton, J.; Martin, J.-L. *J. Phys. Chem. B* **1997**, *101*, 9820.

(15) Lin, S.; Jackson, J.; Taguchi, A. K. W.; Woodbury, N. W. *J. Phys. Chem. B* **1998**, *102*, 4016.

(16) Van Brederode, M. E.; Jones, M. R.; Van Mourik, F.; Van Stokkum, I. H. M.; Van Grondelle, R. *Biochemistry* **1997**, *36*, 6855.

(17) Van Brederode, M. E.; Van Stokkum, I. H. M.; Katilius, E.; Van Mourik, F.; Jones, M. R.; Van Grondelle, R. *Biochemistry* **1999**, *38*, 7545.

(18) Van Brederode, M. E.; Van Mourik, F.; Van Stokkum, I. H. M.; Jones, M. R.; Van Grondelle, R. *Proc. Natl. Acad. Sci. U.S.A.* **1999**, *96*, 2054.

(19) Goldsmith, J. O.; Boxer, S. G. *Biochim. Biophys. Acta* **1996**, *1276*, 171.

(20) Williams, J. C.; Alden, R. G.; Murchison, H. A.; Peloquin, J. M.; Woodbury, N. W.; Allen, J. P. *Biochemistry* **1992**, *31*, 11029.

(21) Nagarajan, V.; Parson, W. W.; Davis, D.; Schenck, C. C. *Biochemistry* **1993**, *32*, 12324.

(22) Andrews, S. S.; Boxer, S. G. *Rev. Sci. Instrum.* **2000**, *71*, 3567.

(23) Bublitz, G. U.; Boxer, S. G. *Annu. Rev. Phys. Chem.* **1997**, *48*, 213.

(24) In Parts 1 and 2, spectra were scaled to an optical density of 1.0 at the peak of the B band. Since many of the mutations in the present study significantly influence the broadness of the B band, we have instead chosen the H band as a standard, even though many of these mutations do influence the H band as well. The absorption and Stark spectra in Parts 1 and 2 should be divided by roughly 4 for comparison with the spectra here.

(25) Steffen, M. A.; Lao, K. Q.; Boxer, S. G. *Science* **1994**, *264*, 810.

(26) Sauer, K.; Dratz, E. A.; Coyne, L. *Proc. Natl. Acad. Sci. U.S.A.* **1968**, *61*, 17.

(27) Lous, E. J.; Hoff, A. J. *Proc. Natl. Acad. Sci. U.S.A.* **1987**, *84*.

(28) Moore, L. J.; Zhou, H. L.; Boxer, S. G. *Biochemistry* **1999**, *38*, 11949.

(29) Jordanides, X. J.; Scholes, G. D.; Fleming, G. R. *J. Phys. Chem. B* **2001**, *105*, 1652.

(30) Kirmaier, C.; Gaul, D.; DeBey, R.; Holten, D.; Schenck, C. C. *Science* **1991**, *251*, 922.

(31) Lockhart, D. J.; Boxer, S. G. *Proc. Natl. Acad. Sci. U.S.A.* **1988**, *85*, 107.

(32) Kropacheva, T. N.; Hoff, A. J. *J. Phys. Chem. B* **2001**, *105*, 5536.

(33) Moss, D. A.; Leonhard, M.; Bauscher, M.; Mantele, W. *FEBS Lett.* **1991**, *283*, 33.

(34) Groot, M.-L.; Yu, J.-Y.; Agarwal, R.; Norris, J. R.; Fleming, G. R. *J. Phys. Chem. B* **1998**, *102*, 5923.

(35) Ermler, U.; Fritzsch, G.; Buchanan, S. K.; Michel, H. *Structure* **1995**, *2*, 925.

(36) Czarnecki, K.; Kirmaier, C.; Holten, D.; Bocian, D. F. *J. Phys. Chem. A* **1999**, *103*, 2235.

(37) For both WT Q_A^- and WT P^+, the 4ω spectral line shape changed significantly upon changing χ; the values of ζ_{CT} determined from their 6ω spectra were close to 45°.

(38) $P(\bar{\nu})$ was used for the Franck−Condon weighted density of states. F^4- through F^{12}-dependent Stark effects were included for the calculation of 4ω spectra; F^6- through F^{16}-dependent Stark effects were included for the calculation of 6ω spectra. In both cases, it was confirmed that the error introduced by truncating the calculation at these terms was insignificant.

(39) Brunschwig, B. S.; Creutz, C.; Sutin, N. *Coord. Chem. Rev.* **1998**, *177*, 61.

(40) It was suggested in Part 2 that the value of Δ_{CT} might be 1600 cm^{-1}, a number that is more consistent with the generally smaller values of $f\Delta\mu_R$ estimated in that study. Using 1600 cm^{-1} for Δ_{CT} for fitting the M203GD spectra more than doubles the sum of the squared residuals for the best fit values of δ, W_R, and $f\Delta\mu_R$ compared to using the value of 1000 cm^{-1} for Δ_{CT}. This revised estimate for the value of Δ_{CT} is favored due to the increased accuracy of the modeling employed in this study.

(41) It is unlikely that the perturbations that we have made to the RCs should significantly affect the value of Δ_{CT} for $B_L^* \rightarrow B_L^+H_L^-$. As described in Part 3 of this series, the value of Δ_{CT}^2 is proportional to the product of the reorganization energy and the mean vibrational frequency of an excited-state charge-transfer process; thus, for example, even a 50% perturbation to the value of one of these parameters will result in only a ~25% perturbation to the value of Δ_{CT}. When we consider that electrostatic perturbations to the reorganization energy and the mean vibrational frequency are not expected to be more than a small fraction of their values,[60] it is highly unlikely that the outer sphere perturbations that we have employed will affect Δ_{CT} significantly.

(42) The mechanism of screening that we have investigated in this manner involves principally the long time scale reorganizations of the protein at room temperature in response to these chemical perturbations.

(43) Reimers, J. R.; Hutter, M. C.; Hughes, J. M.; Hush, N. S. *Int. J. Quantum Chem.* **2000**, *80*, 1224.

(44) Schutz, C. N.; Warshel, A. *Proteins: Struct., Funct., Genet.* **2001**, *44*, 400.

(45) Nagarajan, V.; Parson, W. W.; Gaul, D.; Schenck, C. *Proc. Natl. Acad. Sci. U.S.A.* **1990**, *87*, 7888.

(46) Treynor, T. P.; Andrews, S. S.; Boxer, S. G. *J. Phys. Chem. B* **2003**, *107*, 11230.

(47) Scherer, P. O. J.; Fischer, S. F. *Chem. Phys.* **1989**, *131*, 115.

(48) Treynor, T. P.; Boxer, S. G. Unpublished work.

(49) Zhang, L. Y.; Friesner, R. A. *Proc. Natl. Acad. Sci. U.S.A.* **1998**, *95*, 13603.

(50) Moser, C. C.; Keske, J. M.; Warncke, K.; Farid, R. S.; Dutton, P. L. *Nature (London)* **1992**, *355*, 796.

(51) Consistent with transient absorption experiments that showed no evidence for excited-state charge transfer in the P-less L157VR mutant,[61] we have found no resonance Stark effect in this mutant. Apparently P-less preparations of L157VE and L154LD RCs also exhibit no resonance Stark effects.

(52) Beese, D.; Steiner, R.; Scheer, H.; Angerhofer, A.; Robert, B.; Lutz, M. *Photochem. Photobiol.* **1988**, *47*, 293.

(53) Hartwich, G.; Friese, M.; Scheer, H.; Ogrodnik, A.; Michel-Beyerle, M. E. *Chem. Phys.* **1995**, *197*, 423.

(54) Shochat, S.; Arlt, T.; Francke, C.; Gast, P.; van Noort, P. I.; Otte, S. C. M.; Schelvis, H. P. M.; Schmidt, S.; Vijgenboom, E.; Vrieze, J.; Zinth, W.; Hoff, A. J. *Photosynth. Res.* **1994**, *40*, 55.

(55) Van Brederode, M. E.; Jones, M. R.; Van Grondelle, R. *Chem. Phys. Lett.* **1997**, *268*, 143.

(56) Van Brederode, M. E.; Ridge, J. P.; Van Stokkum, I. H. M.; Van Mourik, F.; Jones, M. R.; Van Grondelle, R. *Photosynth. Res.* **1998**, *55*, 141.

(57) Marcus, R. A.; Sutin, N. *Biochim. Biophys. Acta* **1985**, *811*, 265.

(58) Reimers, J. R.; Hush, N. S. *Chem. Phys.* **1996**, *208*, 177.

(59) Bixon, M.; Jortner, J. *J. Phys. Chem.* **1986**, *90*, 3795.

(60) Treynor, T. P.; Boxer, S. G. *J. Phys. Chem. A* **2004**, *108*, 1764.

(61) Jackson, J. A.; Lin, S.; Taguchi, A. K. W.; Williams, J. C.; Allen, J. P.; Woodbury, N. W. *J. Phys. Chem. B* **1997**, *101*, 5747.

(62) Gunner, M. R.; Dutton, P. L. *J. Am. Chem. Soc.* **1989**, *111*, 3400.

(63) Lin, X.; Murchison, H. A.; Nagarajan, V.; Parson, W. W.; Allen, J. P.; Williams, J. C. *Proc. Natl. Acad. Sci. U.S.A.* **1994**, *91*, 10265.

(64) Lin, X.; Williams, J. C.; Allen, J. P.; Mathis, P. *Biochemistry* **1994**, *33*, 13517.

(65) Bixon, M.; Jortner, J.; Michel-Beyerle, M. E. *Chem. Phys.* **1995**, *197*, 389.

(66) deWinter, A.; Boxer, S. G. *J. Phys. Chem. B* **1999**, *103*, 8786.

(67) Katilius, E.; Turanchik, T.; Lin, S.; Taguchi, A. K. W.; Woodbury, N. W. *J. Phys. Chem. B* **1999**, *103*, 7386.

(68) Reimers, J. R.; Hush, N. S. *J. Am. Chem. Soc.* **2004**, *126*, 4132.